Evaluation of NO_x emissions and ozone production due to vehicular traffic via second-order models

Caterina Balzotti* Maya Briani† Barbara De Filippo† Benedetto Piccoli‡

Abstract

The societal impact of traffic is a long-standing and complex problem. We focus on the estimation of ozone production due to vehicular traffic. For this, we couple a system of conservation laws for vehicular traffic, an emission model, and a system of partial differential equations for the main reactions leading to ozone production. The second-order model for traffic is obtained choosing a special velocity function for a Collapsed Generalized Aw-Rascle-Zhang model and is tuned on NGSIM data. On the other side, the system of partial differential equations describes the main chemical reactions of NO_x gases with a source term provided by a general emission model applied to the output of the traffic model. We analyze the ozone impact of various traffic scenarios and describe the effect of traffic light timing. The numerical tests show the negative effect of vehicles restarts on NO_x emissions, suggesting to increase the length of the green phase of traffic lights to reduce them.

Keywords. Road traffic modeling; second-order traffic models; emissions; ozone production.

Mathematics Subject Classification. 35L65, 90B20, 62P12.

1 Introduction

The impact of road traffic and its inefficiencies on society is well known and was documented with quantitative estimates for more than a decade [29]. Moreover, the societal impact is high also in terms of pollution and environmental effects, with road traffic accounting for nearly one third of carbon dioxide (CO_2) emissions [30]. In general, the impact of air quality on public's health is one of the world's worst toxic pollution problems in this century, the current levels of air pollutants in urban areas are associated with large number of health conditions, including respiratory infections, heart disease [8] and cancer. Air pollutants also contribute to the phenomena of greenhouse effect, ozone depletion, deforestation and the acidification of water and soils [21] and they can induce certain diseases as well as damages on materials (plastic, metals, stones), including Cultural Heritage's ones [28, 7]. While CO_2 is probably one of the most studied molecules, the effect on health is also related to other pollutants, such as particulate matters and nitrogen dioxide (NO_2), see [36]. Here we focus on the production of ozone which stems out of chemical reactions in the atmosphere of the NO_x gases [2, 32].

Much attention has been devoted in traffic literature to quantities such as flow, capacity and travel time. However, advanced modeling of fuel consumption and emission still faces limitations, especially for tools which can be integrated with the increasing flow of data from probe sensors. One of the main reasons is the high variability of fuel consumption and emissions, which are influenced by many factors as the vehicle type, make, model, year and others. Even if the estimation of fuel consumption

*Dipartimento di Scienze di Base e Applicate per l'Ingegneria, Sapienza Università di Roma, Rome, Italy (caterina.balzotti@sbai.uniroma1.it)

†Istituto per le Applicazioni del Calcolo "M. Picone", Consiglio Nazionale delle Ricerche, Rome, Italy (m.briani@iac.cnr.it, b.defilippo@iac.cnr.it)

‡Department of Mathematical Sciences, Rutgers University, Camden, USA (piccoli@camden.rutgers.edu)

and emission at the level of single vehicle presents such drawbacks, as shown in [20], it is possible to achieve reliable estimates using second-order macroscopic models paired with probe sensor data. We thus build-up on this idea by coupling a second-order macroscopic model with a system of ordinary differential equations (briefly ODEs) representing the complex chemical reactions of NO_x gases, still subject to intensive research, which lead to ozone production. Specifically, we propose a tool capable of analyzing the environmental impact of vehicular traffic through three consecutive steps, each powered by the previous one: 1) Estimate of traffic quantities, i.e. density, speed and acceleration of vehicles; 2) Estimate of the emission rates of specific pollutants exploiting the traffic variables; 3) Study of the chemical reactions associated to the pollutant under analysis.

To complete the analysis we should also consider the diffusion in air of pollutants. Some example of reaction-diffusion models using partial differential equations (PDEs) have been proposed in [1, 23, 27]. The inclusion of a further module regarding the atmospheric diffusion of pollutants in our tool is still under investigation.

Let us start by discussing the first step relative to the evaluation of traffic quantities. First notice that most emission models use both the speed v and acceleration a of vehicles [5]. Thus a macroscopic model to be paired with an emission estimator must be of second-order, i.e. consists of an equation for conservation of mass and one for balance of momentum. In particular, the density-flow relation, also known as fundamental diagram, is typically multi-valued and allow a better fit of traffic data. General approaches have been proposed for second-order models [11, 15], extending the well-know Aw-Rascle-Zhang model [4, 35]. The recent paper [10] proposed to use a generalized second-order model with collapsed fundamental diagram in the free phase, thus allowing phase transitions with a simpler description and fitting well with probe and fixed sensor data. This modeling framework is called Collapsed Generalized Aw-Rascle-Zhang Models (briefly CGARZ) and we specify a model in this class by interpolating the Newell-Daganzo or triangular fundamental diagram with the Greenshield quadratic one.

The second step rely on emission models. Among the different models available in literature we have chosen to use the one in [19] based on a combination of velocity, acceleration and their powers, with parameters specifically tuned for NO_x emissions of a petrol car. Then we pass to the third step which consists in modeling the chemical reactions at the base of ozone production in the atmosphere caused from NO_x emissions due to vehicular traffic. Traffic is estimated to cause around one half of nitrogen oxide production, which in turn is one of the main precursor of ozone. The photodissociation of NO_2 is then responsible for the production of the highly reactive O atom and, finally, of ozone. The model capturing these reactions is comprised of a system of five differential equations. The production of NO_2 is tuned to 15% of the overall NO_x production as suggested by the recent work [6]. Since we are mostly interested in the emissions and main reactions at street level, we pair the CGARZ model with simple PDEs derived from the system of ODEs distributed along a one-dimensional parametrization of a road. The ODEs system turns out to be stiff. The CGARZ system is responsible for the source term of the PDEs, representing NO_x emissions. The coupled system is then simulated using a Godunov-type scheme [10] for the CGARZ paired with an ODE-solver for stiff problems for the reactions differential system. The complete procedure is given in Algoritm 1, where we merge the numerical methods for the three modules of our tool. The algorithm works with the time step of the numerical scheme related to the CGARZ model and uses a Matlab ODE-solver with adaptive time step for the system of chemical reactions.

The last but not least part of the paper is devoted to the application of the proposed procedure to various traffic scenarios. The first numerical test is used to validate the emission model. Indeed, first the second-order traffic model is tuned and tested on NGSIM data [31]. Then, as in [20], we compare emission predictions using the CGARZ model and a macroscopic emission formula with *ground-truth* emissions using the whole NGSIM dataset and a microscopic emission formula. The resulting predictions need a correction factor, which is determined alternating the NGSIM data blocks (each of 15 minutes) as training and verification data. The overall relative error ranges between 5% and 23% with an average value of 14%. Notice that the relative error would be on the high end

if the ultimate goal of the investigation would be the exact estimates of the emissions. Finally we analyze the complete procedure which leads to the production of ozone. We first run a simple test: the simulation of an interaction between a shock wave with a rarefaction. The shock represent a backward moving queue while the rarefaction an acceleration wave. The shock has minimal effect on the NO_x emissions while the acceleration wave is the most responsible for the highest values. We then consider a road with a traffic light and green-red cycles. The emissions are compared for different length of the cycle and different proportions of the red-green times. The length of the cycle strongly affects NO_x emissions: moving from 2.5 minutes to 7.5 minutes produces an increase of around 10% of emissions, see Figure 8. On the other side, the variation of the red time versus green one does not affect significantly NO_x emissions, except for an initial ramp up phase when starting from empty road, see Figure 9. These findings are in line with what observed in the first test, but quite different than common intuition. We then focus specifically on ozone production. The overall coupled system of PDEs and ODEs is simulated for 30 minutes corresponding to the two tests without and with the traffic light. The ozone rapidly increases and then reach a linear growth behavior in case of traffic light, while apparently saturate in case of no traffic light. Moreover, the ozone appear to be quite uniformly distributed along the road.

One of the main conclusions of this work is that the duration of traffic cycles affects NO_x emissions and ozone production more than the ratio between green and red phase. Therefore, in order to reduce traffic emissions, a possible solution that emerges from this study is the reduction of vehicle restarts by increasing the green phase duration of traffic lights.

The paper is organized as follows. In Section 2 we describe the CGARZ model and in Section 3 the emission model. In Section 4 we introduce a simplified set of chemical reactions which lead to ozone production. In Section 5 we merge the traffic model with the system of ODEs associated to the chemical reactions, giving an algorithm for the complete numerical procedure. Finally, in Section 6 we propose some numerical tests to estimate the production of ozone.

2 Traffic model

This section is devoted to the first step of our tool: the traffic model. Vehicles dynamics are described by means of a macroscopic second order traffic model, providing the quantities we are interested in, i.e. density, speed and acceleration of vehicles. Specifically, we introduce the *Collapsed Generalized Aw-Rascle-Zhang* (hereafter CGARZ) model [10], to describe the evolution of traffic flow, proposing new flux and velocity functions.

2.1 CGARZ Model

The CGARZ model is one of the *Generic Second Order Models* (GSOM) [15], a family of macroscopic models which satisfy

$$\begin{cases} \rho_t + (\rho v)_x = 0 \\ w_t + v w_x = 0 \end{cases} \qquad \text{with } v = V(\rho, w), \tag{2.1}$$

for a specific velocity function V. The variables $\rho(x,t)$, $v(x,t)$ and $w(x,t)$ are respectively the traffic density, the velocity and a property of vehicles which is advected by traffic flow. The problem can be written in conservative form as:

$$\begin{cases} \rho_t + (\rho v)_x = 0 \\ y_t + (y v)_x = 0 \end{cases} \qquad \text{with } v = V(\rho, y/\rho), \tag{2.2}$$

where $y = \rho w$ is the conserved *total property*. The variable w correlates different behaviors of drivers to the flow-density curves. Thus, the GSOM posses a family of fundamental diagrams $Q(\rho, w) = \rho V(\rho, w)$, parametrized by w. The peculiarity of the CGARZ model is that w does not influence the traffic behavior in the low density regime. This means that vehicles may posses different properties, but the velocity and flow in free-flow is not affected by w. Thus, CGARZ possesses a single-valued fundamental diagram in free-flow, and a multi-valued function in congestion. The flux function has then the following form

$$Q(\rho, w) = \begin{cases} Q_f(\rho) & \text{if } 0 \leq \rho \leq \rho_f \\ Q_c(\rho, w) & \text{if } \rho_f \leq \rho \leq \rho^{\max}, \end{cases} \tag{2.3}$$

where ρ_f is the *free-flow threshold density* independent on w, and $\rho^{\max}$ is the maximum density. Following [10], the flux function (2.3) has to satisfy the following properties:

Q1. $Q(\rho, w) \in C^1$ for each w.

Q2. Flux curves have a common $\rho^{\max}$ independent of w, $Q(\rho^{\max}, w) = 0$, $\forall\, w$.

Q3. The flux is strictly concave with respect ρ, $\frac{\partial^2 Q(\rho,w)}{\partial \rho^2} < 0$ for $\rho \in [0, \rho^{\max})$.

Q4. $\frac{\partial Q(\rho,w)}{\partial w} > 0$ if $\rho_f < \rho < \rho^{\max}$.

The flux function (2.3) defines a velocity function $V(\rho, w) = Q(\rho, w)/\rho$. Thus, as a consequence of the properties of Q, the velocity function V is in C^1 and is strictly decreasing with respect to ρ. Moreover, V satisfies:

V1. Vehicles never go backwards, $V(\rho, w) \geq 0$.

V2. $\rho^{\max}$ is the only density such that $V(\rho^{\max}, w) = 0$.

V3. In the free-flow regime, the traffic velocity is independent of w, $\frac{\partial V(\rho,w)}{\partial w} = 0$ if $0 \leq \rho \leq \rho_f$.

V4. In the congestion regime, the traffic velocity is increasing with respect to w, $\frac{\partial V(\rho,w)}{\partial w} > 0$ if $\rho_f \leq \rho \leq \rho^{\max}$.

In the next section we propose a new family of fundamental diagrams that satisfy the properties listed above.

2.1.1 Flux and velocity functions

Here we make a choice for the flux function of the CGARZ family, thus determining a unique model to be used. Differently from [10], we choose the flux function to be an interpolation between a triangular fundamental diagram, also known as Newell-Daganzo, and a Greenshield fundamental diagram. The reason for this choice is that those two diagrams are the most known and used in traffic modeling and they present two somehow opposite behavior, with the triangular one presenting a unique characteristic speed in congested regime, thus allowing contact discontinuities, while the Greenshield one being genuinely nonlinear in congested regime thus exhibiting rarefaction waves.

The model parameters to be calibrated from data are the following: the maximum speed $V^{\max}$, the threshold density ρ_f from the free-flow to the congested phase, the density ρ_c in which the flux function reaches his maximum value, and a lower and upper bound for w, denoted by w_L and w_R respectively. Moreover, we set the maximal density $\rho^{\max}$ as a property of the road.
As in [10], we assume the Greenshields model in the free-flow regime, i.e.

$$Q_f(\rho) = \rho V^{\max} \left(1 - \frac{\rho}{\rho^{\max}}\right),$$

and as a novelty we define the flux function $Q_c(\rho, w)$ in the congested phase, as a convex combination of a lower-bound function $f(\rho)$ and an upper-bound function $g(\rho)$. In particular, we set

$$f(\rho) = \rho_f V^{\max}\left(1 - \frac{\rho}{\rho^{\max}}\right) \tag{2.4}$$

as the straight-line which connects $(\rho_f, Q_f(\rho_f))$ with $(\rho^{\max}, 0)$, and

$$g(\rho) = \rho V^{\max}\left(1 - \frac{\rho}{\rho^{\max}}\right) \tag{2.5}$$

which corresponds to the free-flow phase flux function. Defining

$$\lambda(w) = \frac{w - w_L}{w_R - w_L}, \tag{2.6}$$

then our flux function $Q_c(\rho, w)$ is

$$Q_c(\rho, w) = (1 - \lambda(w))f(\rho) + \lambda(w)g(\rho),$$

with f and g given in (2.4) and (2.5) respectively. The resulting flux function is

$$Q(\rho, w) = \begin{cases} \rho V^{\max}\left(1 - \frac{\rho}{\rho^{\max}}\right) & \text{if } 0 \le \rho \le \rho_f \\ (1 - \lambda(w))f(\rho) + \lambda(w)g(\rho) & \text{if } \rho_f \le \rho \le \rho^{\max}. \end{cases} \tag{2.7}$$

Proposition 1. *The flux function (2.7) verifies the properties Q2-Q4 and the property Q1 for all $\rho \neq \rho_f$.*

Proof. The function Q is $\mathcal{C}^1$ in $[0, \rho^{\max}]\backslash\{\rho_f\}$ by construction: the free-flow part Q_f is $\mathcal{C}^1$ for all ρ, and the congested one is a convex combination of $\mathcal{C}^1$ functions. Condition Q2 follows directly from the definition of f and g which satisfy $f(\rho^{\max}) = g(\rho^{\max}) = 0$. Condition Q3 is easily verified by the strictly negativity of the second derivative of function in (2.7). Finally, condition Q4 follows from the relation

$$\frac{\partial Q(\rho, w)}{\partial w} = \lambda'(w)(g(\rho) - f(\rho))$$

which is strictly positive since $g(\rho) > f(\rho)$ by construction. □

Remark 2.1. *To verify condition Q1 for all $\rho \in [0, \rho^{\max}]$, it is sufficient to choose a different function f that joins with regularity to free-flow regime.*

Once the flux function is defined, the velocity function is obtained as

$$V(\rho, w) = \frac{Q(\rho, w)}{\rho}. \tag{2.8}$$

2.1.2 Acceleration function

In time-continuous second-order models, the acceleration equation is a second partial differential equation of the general form

$$\frac{Dv(x,t)}{Dt} = (v_t(x,t) + v(x,t)v_x(x,t)) = a(\rho(x,t), v(x,t)),$$

where $\frac{D\cdot}{Dt}$ is the total derivative and v is the speed function. This equation implies that the rate of change of the local speed $\frac{Dv(x,t)}{Dt} = (v_t + vv_x)$ in Lagrangian coordinates is equal to an *acceleration function* $a(x,t) = a(\rho(x,t), v(x,t))$.

In CGARZ model we derive the function acceleration by computing the total derivative of $V(\rho, w)$, i.e.

$$a(x,t) = \frac{Dv(x,t)}{Dt} = v_t(x,t) + v(x,t)v_x(x,t),$$

where $v(x,t) = V(\rho(x,t), w(x,t))$, $v_t = V_\rho \rho_t + V_w w_t$, $v_x = V_\rho \rho_x + V_w w_x$. Then,

$$a(x,t) = (\rho_t + v\rho_x)\, V_\rho + (w_t + vw_x)\, V_w,$$

and by applying the homogeneous equation in (2.1) for w we get

$$a(x,t) = V_\rho\, (\rho_t + v\rho_x) = -V_\rho \rho v_x. \tag{2.9}$$

3 Estimating emissions by traffic quantities

In this section we analyze the second step of our tool: the emission model. Specifically, we describe the emission model proposed in [19] appropriate for several air pollutants. Emitted by different sources, primary and secondary air pollutants mainly include: sulphur oxides (SO_x), nitrogen oxides (NO_x), volatile organic compounds (VOC), particulates (PM), free radicals, toxic metals, etc. [33, 24]. In areas with heavy street traffic and high amounts of UV radiation, ozone (O_3), NO_x and hydrocarbons (HC) are of particular interest.

The existence of high concentration of ozone in the urban atmosphere suggests to have an effective control of some other pollutants such as carbon monoxide (CO) and sulphur dioxide (SO_2), ozone is a secondary pollutant formed in the ambient air through a complex set of sunlight initiated reactions of its precursor, primary emission of VOC, catalyzed by hydrogen oxide radicals, and of NO_x [12, 26]. For the complexity of the phenomena involved, in this paper we focus on emission models for only NO_x.

3.1 Emission Model

We use the microscopic emission model proposed in [19]. This model gives the instantaneous emission rate of four pollutant types: carbon dioxide, nitrogen oxides, volatile organic compounds and particulate matter. The emission rate E_i of vehicle i at time t is computed using vehicle's instantaneous speed $v_i(t)$ and acceleration $a_i(t)$

$$E_i(t) = \max\{E_0, f_1 + f_2 v_i(t) + f_3 v_i(t)^2 + f_4 a_i(t) + f_5 a_i(t)^2 + f_6 v_i(t) a_i(t)\}, \tag{3.1}$$

where E_0 is a lower-bound of emission and f_1 to f_6 are emission constants. The parameters are experimentally calibrated using non-linear multiple regression techniques as explained in [19]. Both the emission lower-bound and coefficients differ according to the type of pollutant and of vehicle (i.e. petrol car, diesel car, truck, etc.). We are particularly interested in the NO_x emission rate, whose coefficients depend on whether the vehicle is in acceleration (defined as $a_i(t) \geq -0.5$ m/s^2) or deceleration (with $a_i(t) < -0.5\,\mathrm{m/s^2}$) mode, where m denotes meter and s second. In Table 1 we report the NO_x emission coefficients for a petrol car, for which $E_0 = 0$. See [19, Table 2] for the coefficients related to the other pollutants and vehicles type.

Remark 3.1. *In this work we assume to have a unique typology of vehicles, i.e. petrol cars. The integration with other types of vehicles and comparison of the corresponding emission rates is an interesting subject of study, it would require the use of traffic models for multi-class vehicles and this goes beyond the scope of this work.*

Assuming to have N vehicles in a stretch of road going all at the same speed $\bar{v}$, with the same acceleration $\bar{a}$, the emission rate is given by the N contributes of the vehicles, such that

$$E(t) = \sum_{i=1}^{N} E_i(t) = N \max\{E_0, f_1 + f_2 \bar{v}(t) + f_3 \bar{v}(t)^2 + f_4 \bar{a}(t) + f_5 \bar{a}(t)^2 + f_6 \bar{v}(t)\bar{a}(t)\}. \tag{3.2}$$

Vehicle mode	$f_1\ \left[\frac{\mathrm{g}}{\mathrm{s}}\right]$	$f_2\ \left[\frac{\mathrm{g}}{\mathrm{m}}\right]$	$f_3\ \left[\frac{\mathrm{g\,s}}{\mathrm{m}^2}\right]$	$f_4\ \left[\frac{\mathrm{g\,s}}{\mathrm{m}}\right]$	$f_5\ \left[\frac{\mathrm{g\,s}^3}{\mathrm{m}^2}\right]$	$f_6\ \left[\frac{\mathrm{g\,s}^2}{\mathrm{m}^2}\right]$
If $a_i(t) \geq -0.5\,\mathrm{m/s}^2$	6.19e-04	8e-05	-4.03e-06	-4.13e-04	3.80e-04	1.77e-04
If $a_i(t) < -0.5\,\mathrm{m/s}^2$	2.17e-04	0	0	0	0	0

Table 1. NO_x parameters in emission rate formula (3.1) for a petrol car, where g denotes gram, m meter and s second.

In particular this equation can be used in conjunction with quantities provided by a numerical solution to a macroscopic model such as the CGARZ one.

Remark 3.2. *We make use of a particular emission model. However, the large majority of microscopic emissions models are based on a combination of polynomial expression in the velocity and acceleration, see for instance* [5, 25] *and references therein. Thus our analysis can be easily adapted to other models.*

4 Chemical reactions

This section is devoted to the final step of our tool: the chemical reactions associated to the pollutants under investigation. In particular, in this work we focus on NO_x gases and the reactions which lead to the O_3 formation. NO_x gases are usually produced from the reaction among nitrogen and oxygen (O_2) during combustion of fuels, such as hydrocarbons, in air, especially at high temperatures, such as occurs in car engines [18]. They include nitrogen oxide (NO) and nitrogen dioxide (NO_2), the latter is classified as a secondary pollutant. NO is produced according to the following reaction with O_2 and nitrogen (N_2) [17],

$$N_2 + O_2 \longrightarrow 2NO,$$

where the rate of the chemical reaction can be increased by raising the temperature. In the combustion mechanism, NO can react with O_2 thus forming NO_2,

$$2NO + O_2 \longrightarrow 2NO_2.$$

NO_2 is a very reactive compound that can be photo-dissociated into atomic oxygen (O), this mechanism is considered one of key steps in the formation of tropospheric ozone [3]. Nitrogen oxides and volatile organic compounds are considered ozone precursors, where traffic is considered the main source (more than 50% of anthropogenic source). The photolysis of NO_2 is speeded up in warmer conditions and with more UV-light. In the troposphere with strong solar irradiation, NO_2 is a relevant precursor substance for the ozone in photochemical smog and it is due to the following reactions:

$$NO_2 + h\nu \xrightarrow{k_1} O + NO \tag{4.1}$$

$$O + O_2 + M \xrightarrow{k_2} O_3 + M, \tag{4.2}$$

where h is Planck's constant, ν its frequency and k_1, k_2 are the reaction rate constants. M is a chemical species, such as O_2 or N_2, that adsorbs the excess of energy generated in reaction (4.2) [17]. Moreover, in presence of NO, O_3 reacts with it and this reaction destroys the ozone and reproduces the NO_2, with kinetic constant k_3:

$$O_3 + NO \xrightarrow{k_3} O_2 + NO_2. \tag{4.3}$$

This means that the previous reactions do not result net ozone production, because the reactions only recycle O_3 and NO_x. Net ozone production occurs, when other precursors, such as carbon

monoxide, methane, non-methane hydrocarbons or certain other organic compounds (volatile organic compounds) are present in the atmosphere and fuel the general pathways to tropospheric O_3 formation. Although it would be interesting to consider the whole ground-level ozone production, here we focus only on the photochemical smog reactions (4.1), (4.2) and (4.3).

For vehicle's emissions, the maximum NO_2 concentration is recorded at medium engine load and low engine speed. At high speed, the NO_2 emissions are reduced to a minimum (in most cases less than 4%) [22]. According to a recent study using British data [6], the fraction of NO_2 in vehicle NO_x emissions (all fuels) increased from around 5-7% in 1996 to 15-16% in 2009. For this reason we will consider in our simulation a NO_2 concentration equal to 15% of NO_x.

Now, we set up the system of ordinary differential equations associated to the chemical reactions (4.1), (4.2) and (4.3). We assume that the reactions take place in a volume of dimension Δx^3, during the daily hours and that the chemical specie M in (4.2) is O_2. Moreover, we add the traffic emissions contribution as a source term for the concentration of NO and NO_2. Hence, we denote the chemical species concentration by $[\cdot] = [\frac{\text{weight unit}}{\text{volume unit}}]$ and we define the variation of the concentration of NO_x in Δx^3, at each time t as

$$S_{NO_x} = \frac{E_{NO_x}(t)}{\Delta x^3}, \tag{4.4}$$

where the emission rate $E_{NO_x}(t)$ is given by (3.2).

The final system of equations, given by coupling the three reactions (4.1)-(4.3) and the source term (4.4), becomes

$$\begin{aligned}
d[O]/dt &= -k_2[O]\,[O_2]^2 + k_1[NO_2] \\
d[O_2]/dt &= -k_2[O]\,[O_2]^2 + k_3[O_3]\,[NO] \\
d[O_3]/dt &= k_2[O]\,[O_2]^2 - k_3[O_3]\,[NO] \\
d[NO]/dt &= k_1[NO_2] - k_3[O_3]\,[NO] + (1-p)\,S_{NO_x} \\
d[NO_2]/dt &= -k_1[NO_2] + k_3[O_3]\,[NO] + p\,S_{NO_x},
\end{aligned} \tag{4.5}$$

where $p = 0.15$ corresponding to 15% of NO_2 derived from the emission rate of NO_x, and the parameters k_1, k_2 and k_3, shown in Table 2, are estimated according to [13].

k_1	k_2	k_3
$0.02\,s^{-1}$	$6.09 \times 10^{-34}\,cm^6\,molecule^{-2}\,s^{-1}$	$1.81 \times 10^{-14}\,cm^3\,molecule^{-1}\,s^{-1}$

Table 2. Parameters k_1, k_2, and k_3 of system (4.5), where cm denotes centimeter, s second and molecule the number of molecules.

5 From traffic quantities to the production of the ozone

In this section we merge the traffic model with air pollutants dynamics, summarizing the three steps of the proposed tool and introducing the numerical methodology. The procedure is the following:

1. Estimate the traffic quantities, i.e. the density and the speed of vehicles with the CGARZ model (2.2) and the analytical acceleration with (2.9).

2. Estimate the emission rate with (3.2) and the corresponding source term in the chemical reactions per unit of volume given by (4.4).

3. Solve system (4.5) to estimate the chemical species concentration per unit of volume.

We now describe the numerical implementation used for the three modules. Let us consider the space and time domain $[0,L]\times[0,T]$ discretized via a grid of $N_x \times N_t$ cells of length $\Delta x \times \Delta t$. For each cell centered at x_j and time t^n of the numerical grid our aim is then to estimate the traffic quantities ρ_j^n, v_j^n, a_j^n, the emission rates E_j^n, the source term s_j^n and the concentration of the five chemical species $\{(\psi_i)_j^n)\}_{i=1,\dots,5}$, where $\psi_1(x,t)=[\mathrm{O}]$, $\psi_2(x,t)=[\mathrm{O_2}]$, $\psi_3(x,t)=[\mathrm{O_3}]$, $\psi_4(x,t)=[\mathrm{NO}]$ and $\psi_5(x,t)=[\mathrm{NO_2}]$.

5.1 Numerical method for the CGARZ model

The CGARZ model (2.2) is numerically solved using the 2CTM scheme described in [10], which is a Godunov type scheme and can be used for any GSOM. Here we describe the general scheme and how to apply it to the CGARZ model.

Let us consider the numerical grid introduced above and set $v_j^n = V(\rho_j^n, w_j^n)$. The 2CTM scheme is described by the system

$$\rho_j^{n+1} = \rho_j^n - \frac{\Delta t}{\Delta x}(F_{j+1/2}^{\rho,n} - F_{j-1/2}^{\rho,n})$$
$$y_j^{n+1} = y_j^n - \frac{\Delta t}{\Delta x}(F_{j+1/2}^{y,n} - F_{j-1/2}^{y,n}),$$

where $F_{j\pm1/2}^{\rho,n}$ and $F_{j\pm1/2}^{y,n}$ are the numerical fluxes. In order to define $F_{j-1/2}^{\rho,n}$ and $F_{j-1/2}^{y,n}$, consider the two constant left and right states $(\rho^-,w^-)=(\rho_{j-1}^n, w_{j-1}^n)$ and $(\rho^+,w^+)=(\rho_j^n,w_j^n)$ respectively, and compute the solution of the Riemann problem between the two consecutive cells centered in x_{j-1} and x_j,

$$\begin{cases} \rho_t + (\rho v)_x = 0 \\ y_t + (yv)_x = 0 \end{cases} \quad \text{with} \quad (\rho_0, y_0) = \begin{array}{ll} (\rho^-, \rho^- w^-) & \text{if } x < x_{j-1/2} \\ (\rho^+, \rho^+ w^+) & \text{if } x \geq x_{j-1/2}. \end{array}$$

The solution of the Riemann problem is defined by an intermediate state (ρ^*,w^*) separated from the left and right state by a 1-shock or rarefaction wave and a 2-contact discontinuity respectively. The Riemann invariants [9] $w = const.$ and $V(\rho,w) = const.$, imply that $w^* = w^-$ and $V(\rho^*,w^*) = \min\{v^+, V(0,w^-)\}$ with $v^+ = V(\rho^+,w^+)$. Note that the minimum between the two velocities is required since vehicles from the left try to adapt their velocity to v^+, but if $v^+ > V(0,w^-)$ they cannot exceed their maximum speed $V(0,w^-)$. Let introduce now the supply and demand functions S and D defined as

$$S(\rho,w) = \begin{cases} Q^{\max}(w) & \text{if } \rho \leq \rho^{cr}(w) \\ Q(\rho,w) & \text{if } \rho > \rho^{cr}(w) \end{cases} \qquad D(\rho,w) = \begin{cases} Q(\rho,w) & \text{if } \rho \leq \rho^{cr}(w) \\ Q^{\max}(w) & \text{if } \rho > \rho^{cr}(w), \end{cases}$$

with $\rho^{cr}(w)$ critical density, i.e. the value where the flux curve identified by w attends its maximum $Q^{\max}(w)$. The numerical flux is then defined as

$$F_{j-1/2}^{\rho,n} = \min\{D(\rho_{j-1}^n, w_{j-1}^n), S(\rho_{j-1/2}^n, w_{j-1/2}^n)\} \tag{5.1}$$

where $(\rho_{j-1/2}^n, w_{j-1/2}^n)$ is the value of the intermediate state described above. Moreover, since $y=\rho w$ the numerical fluxes $F_{j\pm1/2}^{y,n}$ are such that

$$F_{j-1/2}^{y,n} = w_{j-1/2}^n F_{j-1/2}^{\rho,n} \qquad \text{and} \qquad F_{j+1/2}^{y,n} = w_j^n F_{j+1/2}^{\rho,n}.$$

By construction of the flux function for the CGARZ model, the condition $v^+ > V(0,w^-)$ never holds, since $V(0,w) = V^{\max}$ for any w. Hence the intermediate state (ρ^*,w^*) is such that $w^* = w^-$ and $V(\rho^*,w^*) = v^+$. In (5.1) we then get $w_{j-1/2}^n = w_{j-1}^n$ and $\rho_{j-1/2}^n$ such that $V(\rho_{j-1/2}^n, w_{j-1}^n) = V(\rho_j^n, w_j^n)$.
The stability of the scheme is guaranteed by the CFL condition

$$\Delta t \leq \Delta x/(2\Lambda) \tag{5.2}$$

with $\Lambda = \max_{j=1,2} |\lambda_j|$ and λ_j eigenvalues of the Jacobian matrix associated to (2.2). In our case Λ coincides with the maximum velocity $V^{\max}$.

5.1.1 Evaluating the acceleration

As described in Section 2.1.2, we can approximate the acceleration directly derived from the theoretical model by (2.9) as

$$a_j^n = -V_\rho(\rho_j^n, w_j^n)\rho_j^n \frac{v_{j+1}^n - v_{j-1}^n}{2\Delta x}. \tag{5.3}$$

Here we also describe a discrete formulation for the acceleration recovered by average quantities, as an alternative to (5.3). We follow the approach proposed in [16, 34] for the particular case of a single road with n_ℓ lanes. To define the average acceleration of a cell, we distinguish between the *temporal acceleration* and the *spatial-temporal acceleration*. The temporal acceleration refers to the change of the average speed for the vehicles which remain in the same cell i between time t^n and t^{n+1},

$$a_j^{tmp}(n) = \frac{v_j^{n+1} - v_j^n}{\Delta t}. \tag{5.4}$$

Let q_j^n be the flux of vehicles which cross the cell j between time t^n and t^{n+1}. The total number of vehicles which remain in the cell and therefore which are subjected to the temporal acceleration is $c_j^{tmp}(n) = n_\ell \Delta x \rho_j^n - \Delta t q_j^n$. The spatial-temporal acceleration refers to the change of the average speed for the vehicles which move from a cell to the following one. It is defined as

$$a_j^{spt}(n) = \frac{v_{j+1}^{n+1} - v_j^n}{\Delta t}, \tag{5.5}$$

and the total number of vehicles subjected to this acceleration is $c_j^{spt}(n) = \Delta t q_j^n$. Combining the definitions of temporal (5.4) and spatial-temporal (5.5) acceleration, we can introduce the average acceleration of vehicles in cell j at time t^n as

$$a_j^n = \frac{a_j^{tmp}(n)c_j^{tmp}(n) + a_j^{spt}(n)c_j^{spt}(n)}{c_j^{tmp}(n) + c_j^{spt}(n)},$$

which, after some computations, can be rewritten as

$$a_j^n = \frac{v_j^{n+1} - v_j^n}{\Delta t} + v_j^n \frac{v_{j+1}^{n+1} - v_j^{n+1}}{\Delta x}. \tag{5.6}$$

Hereafter we refer to this formulation as discrete acceleration.

5.2 Numerical method for the system of chemical reactions

The final step of our procedure is the resolution of system (4.5), which gives us the concentration of the chemical species. We rewrite the system as

$$\begin{cases} \partial_t \psi_1(x,t) = k_1\, \psi_5(x,t) - k_2\, \psi_1(x,t)\, \psi_2^2(x,t) \\ \partial_t \psi_2(x,t) = k_3\, \psi_3(x,t)\, \psi_4(x,t) - k_2\, \psi_1(x,t)\, \psi_2^2(x,t) \\ \partial_t \psi_3(x,t) = k_2\, \psi_1(x,t)\, \psi_2^2(x,t) - k_3\, \psi_3(x,t)\, \psi_4(x,t) \\ \partial_t \psi_4(x,t) = k_1\, \psi_5(x,t) - k_3\, \psi_3(x,t)\, \psi_4 + (1-p)s(x,t) \\ \partial_t \psi_5(x,t) = k_3\, \psi_3(x,t)\, \psi_4(x,t) - k_1\, \psi_5(x,t) + ps(x,t), \end{cases} \tag{5.7}$$

with $s(x,t)$ source term defined in (4.4) and $p = 0.15$. System (5.7) in vectorial form is

$$\partial_t \Psi(x,t) = G(t, \Psi(x,t)) \tag{5.8}$$

with $\Psi = (\psi_1, \psi_2, \psi_3, \psi_4, \psi_5)$. First of all we analyze the stiffness of (5.8), see e.g. [14, Chapter 6], without source term, i.e. $s(x,t) = 0$. Therefore, we consider the linearization of G in a neighbourhood of the initial data $\Psi^0 = \Psi(x,0)$. The eigenvalues of the Jacobian of G range in a large interval of values, due to the order of magnitude of chemical species and reaction coefficients k_1, k_2 and k_3 (see Table 2). In particular, we have λ_1 with order of magnitude 10^7, λ_2 of 10^1 and $\lambda_3 = \lambda_4 = \lambda_5 = 0$. A similar result is obtained adding the source term $s(x,t) \neq 0$. Hence, the problem is stiff and we need to approximate system (5.8) with an adaptive step size method. To this end we solve (5.8) using the standard Matlab tool `ode23s`, which makes use of modified Rosenbrock formula of order 2 and works with an adaptive step size.

5.3 Final Algorithm

We are now able to give the unique tool which estimates the concentration of pollutants related to vehicular traffic, collecting the numerical methodologies proposed above. Starting from the initial data

$$(\rho_j^0, y_j^0, (\psi_1)_j^0, (\psi_2)_j^0, (\psi_3)_j^0, (\psi_4)_j^0, (\psi_5)_j^0)$$

and according to suitable boundary conditions, for each $n = 1, \dots, N_t$ and $j = 0, \dots, N_x$ our procedure is summed up in Algorithm 1, with time step Δt satisfying (5.2). We recall that $F^{\rho,n}_{j-1/2}$ is defined in (5.1), the analytical acceleration formula in (2.9) and the emission formula in (3.2) with coefficients f_1 to f_6 reported in Table 1.

Algorithm 1 Pseudocode of the complete procedure

Input: Traffic state and concentration of the 5 chemical species at initial time $t = t^0 = 0$.
Output: Traffic state, NO_x emissions and concentration of the 5 chemical species at final time $t = T$.

for $n = 1$ `to` N_t **do**
  for $j = 0$ `to` N_x **do**
    $\rho_j^{n+1} = \rho_j^n - \dfrac{\Delta t}{\Delta x}(F^{\rho,n}_{j+1/2} - F^{\rho,n}_{j-1/2})$
    $y_j^{n+1} = y_j^n - \dfrac{\Delta t}{\Delta x}(w_j^n F^{\rho,n}_{j+1/2} - w_{j-1}^n F^{\rho,n}_{j-1/2})$
    $w_j^n = \dfrac{y_j^n}{\rho_j^n}$
    $v_j^n = V(\rho_j^n, w_j^n)$
    $a_j^n = -V_\rho(\rho_j^n, w_j^n)\rho_j^n \dfrac{v_{j+1}^n - v_{j-1}^n}{2\Delta x}$ ▷ It can be replaced by (5.6).
    $E_j^n = \rho_j^n \Delta x \ \max(E_0, f_1 + f_2 v_j^n + f_3 (v_j^n)^2 + f_4 a_j^n + f_5 (a_j^n)^2 + f_6 v_j^n a_j^n)$
    $s_j^n = \dfrac{E_j^n}{\Delta x^3}$
    $\Psi_j^{n+1} = \text{ODEsolver}(\Psi_j^n, s_j^n)$ ▷ It uses an adaptive time step size.
  end for
end for

6 Numerical tests

In this section we show some examples illustrating the several steps which lead to the estimate of the production of ozone. First of all we validate the emission model to estimate the NO_x emission

rates with a numerical test using the NGSIM dataset [31]. Then we provide some tests related to the complete procedure, focusing on the production of ozone. In particular, we investigate the impact of traffic lights on pollutants production, looking for strategies to reduce it.

6.1 Validation of the emission model

In this section we compare the NO_x emission rates given by (3.1) computed using the NGSIM dataset [31] with that given by (3.2) computed along numerical solutions to the CGARZ model. In other words, the macroscopic CGARZ model is fed by real data only at initial time, then the emission rate is computed along the numerical solution to CGARZ and compared with that resulting from the NGSIM complete dataset, considered as a *ground truth.*

The NGSIM database contains detailed vehicle trajectory data on the interstate I-80 in California, on April 13, 2005. The area under analysis is approximately 500 meters in length and consists of six freeway lanes. Several video cameras recorded vehicles moving through the monitored area, while a specific software has transcribed the vehicle trajectory data from video. The data include the precise location, velocity and acceleration of each vehicle within the study area every 0.1 seconds. The period analyzed in this work refers to three time slots: 4:00 pm - 4:15 pm, 5:00 pm - 5:15 pm and 5:15 pm - 5:30 pm.

First of all we estimate the flow-density and velocity-density relationships from the dataset. We divide the study area into space-time cells $C_i^n = [x_i, x_{i+1}] \times [t^n, t^{n+1}]$ of length $120\,\mathrm{m} \times 4\,\mathrm{s}$. The density in C_i^n is equal to the number of vehicles (denoted by veh) which cross the cell during the time interval $[t^n, t^{n+1}]$. The velocity in C_i^n is the mean of all the velocities measured in the cell, and the flux is the product between density and velocity. The relationships between flow and density and between velocity and density are shown in the top panels of Figure 1. In the two graphs we clearly see two "clouds" in which data are concentrated (except a small number of outliers accounting for less than 3% of points). From the analysis of these data we have estimated a possible set of model parameters: $V^{\max} = 65\,\mathrm{km/h}$, $\rho_f = 110\,\mathrm{veh/km}$, $\rho^{\max} = 800\,\mathrm{veh/km}$, $\rho_c = \rho^{\max}/2$, $w_L = 5687$ and $w_R = 13000$, where km denotes kilometer, h hour and veh the number of vehicles. Specifically, the parameters $V^{\max}$ and ρ_f are chosen such that the area enclosed between the curves f and g covers more than the 97% of data points of the real data clouds; $\rho^{\max}$ is a property of the road, defined by

$$\rho^{\max} = \frac{\text{Number of lanes}}{\text{Lenght of vehicles}} = \frac{6}{7.5 \times 10^{-3}\,\mathrm{km}},$$

and we set the two extreme w_L and w_R as $w_L = g(\rho_f)$ and $w_R = g(\rho_c)$. The family of curves generated by the data set given above are shown in the bottom panels of Figure 1.

We now focus on NO_x emissions. The microscopic speed and acceleration included in the NGSIM dataset can be fed directly in (3.1) providing microscopic NO_x emissions produced by each vehicle. Then, we sum the emissions of vehicles along the entire road

$$E^{\text{true}}(t^n) = \sum_{i=1}^{N_{car}(t^n)} E_i(t^n), \tag{6.1}$$

where $N_{car}(t^k)$ is the number of vehicles crossing the road at time t^n and $E_i(t^n)$ is the emission rate of vehicle i at time t^n.

The CGARZ model (2.2), calibrated with the NSGIM dataset, is used here to estimate the average density and speed of vehicles along the road. The initial density ρ_0 and velocity v_0 are obtained with a kernel density estimation of the ground-truth data, specifically the Parzen-Rosenblatt window method. Given a vehicle location $x_i(t)$ and velocity $v_i(t)$, density and flow rate functions are obtained as superpositions of Gaussian profiles,

$$\rho(x,t) = \frac{1}{h}\sum_{i=1}^{n} K(x, x_i), \quad v(x,t) = \frac{\sum_{i=1}^{n} v_i K(x, x_i)}{\sum_{i=1}^{n} K(x, x_i)}, \tag{6.2}$$

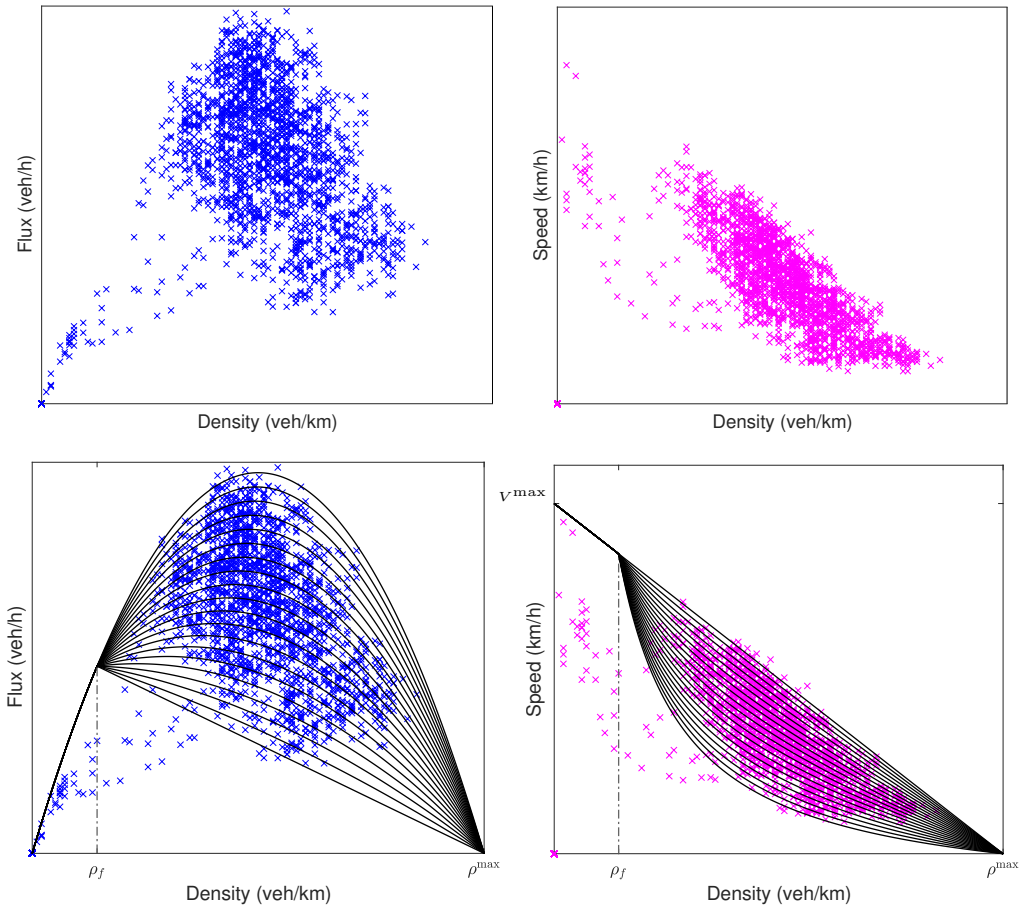

Figure 1. Top: Flow-density relationship (left) and velocity-density relationship (right) from the NGSIM dataset. Bottom: Family of flux functions (2.7) (left) and family of velocity functions (2.8) (right) for the calibrated parameters.

where $K(x, x_i) = \phi((x - x_i)/h) + \phi((x - (2a - x_i))/h) + \phi((x - (2b - x_i))/h)$, $\phi(x) = \exp(-x^2/2)/\sqrt{2\pi}$, h is a distance parameter, a and b are the extremes of the road. In this work $h = 25\,\text{m}$.

The initial w_0 is defined such that $V(\rho_0(x_j), w_0(x_j)) = v_0(x_j)$, for $j = 1, \ldots, N_x$ and then $y_0(x_j) = \rho_0(x_j)w_0(x_j)$. Following the numerical procedure described in Sections 5.1 we compute the average emission rate E_j^n of the cell x_j at time t^n, for all j and n, by means of (3.2). Similar to microscopic case (6.1), we sum the emission rates all over the cells

$$E^{\text{mod}}(t^n) = \sum_{j=1}^{N_x} E_j^n, \tag{6.3}$$

where $t^n = n\delta t$, with $\delta t = 0.1\,\text{s}$ is the time frame of the NGSIM dataset.

Two formulas to compute the acceleration were proposed in (2.9) and (5.6). The first is analytical and adapted for macroscopic models, while the second is discrete and can be used to any type of data. In Figure 2 we compare the numerical results using the two formulations. The red-solid line of the left plot represents the NO_x emission rate computed using the discrete acceleration on average density and speed values obtained via kernel density estimation (6.2) from NGSIM trajectory data. The blue-circles line, instead, represents the ground-truth emission rate (6.1). The results are quite similar,

suggesting the accuracy of the discrete acceleration (5.6). Finally, on the right plot of Figure 2 we compare the emission rate of NO_x computed with equation (3.2), using the two different definitions of the acceleration function (2.9) and (5.6). The results are almost identical and have same computational cost, and this further certifies the efficiency of the CGARZ model (2.2) and suggests the use of the analytical formula (2.9) to estimate emissions.

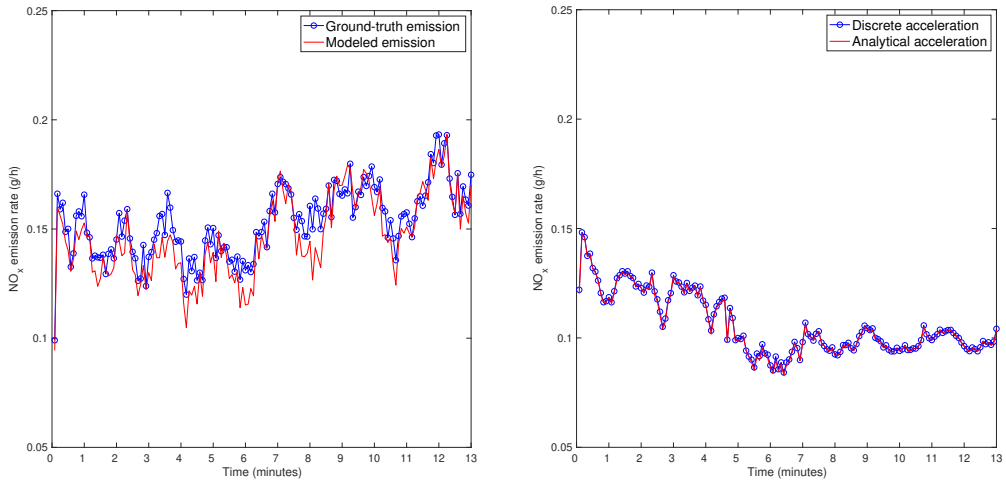

Figure 2. Comparison between ground-truth emission rate and modeled emission rate computed using discrete acceleration (5.6) on density and speed via kernel density estimation (left). Comparison of emission rate computed with the discrete (5.6) and analytical (2.9) acceleration (right). Both the results refer to 500 meters of road and 13 minutes of simulation (data from 4:01 pm - 4:14 pm of NGSIM dataset).

We compare now the emission rate along the entire road obtained with (6.1) and (6.3) respectively, for each period of the NGSIM dataset. The results are computed with 13-minute simulations, in which we exclude the first and the last minute of recorded trajectories for corruption of data. In Figure 3 we observe that the emission rate obtained by the CGARZ model (6.3) (black-dotted) is lower than the ground-truth emission (6.1) (blue-solid). Improved results are obtained by multiplying the modeled emissions by a proper correction factor (red-circles). Specifically, for each data period j, we have computed a correction factor r_j via linear regression between the ground-truth emission and the modeled one. Moreover, we define the following error

$$\text{Error}(r_j) = \frac{\left\| E^{\text{true}} - r_j E^{\text{mod}} \right\|_{L^1}}{\left\| E^{\text{true}} \right\|_{L^1}}, \qquad j = 1, 2, 3, \tag{6.4}$$

where E^{true} and E^{mod} are vectors whose k-th components are given by (6.1) and (6.3) respectively. Table 3 shows the errors (6.4) obtained using the three different correction factors for all the time periods of the NSGIM dataset, where $r_1 = 1.42$, $r_2 = 1.35$ and $r_3 = 1.15$. We observe that the correction factors r_1, r_2 and r_3 give similar results.

Period	Error(r_1)	Error(r_2)	Error(r_3)
4:01 pm - 4:14 pm	0.1604	0.1666	0.2204
5:01 pm - 5:14 pm	0.0819	0.0842	0.1625
5:16 pm - 5:29 pm	0.2304	0.1773	0.0586

Table 3. Errors given by (6.4) for the three slots of the NGSIM dataset and different correction factor $r_1 = 1.42$, $r_2 = 1.35$ and $r_3 = 1.15$.

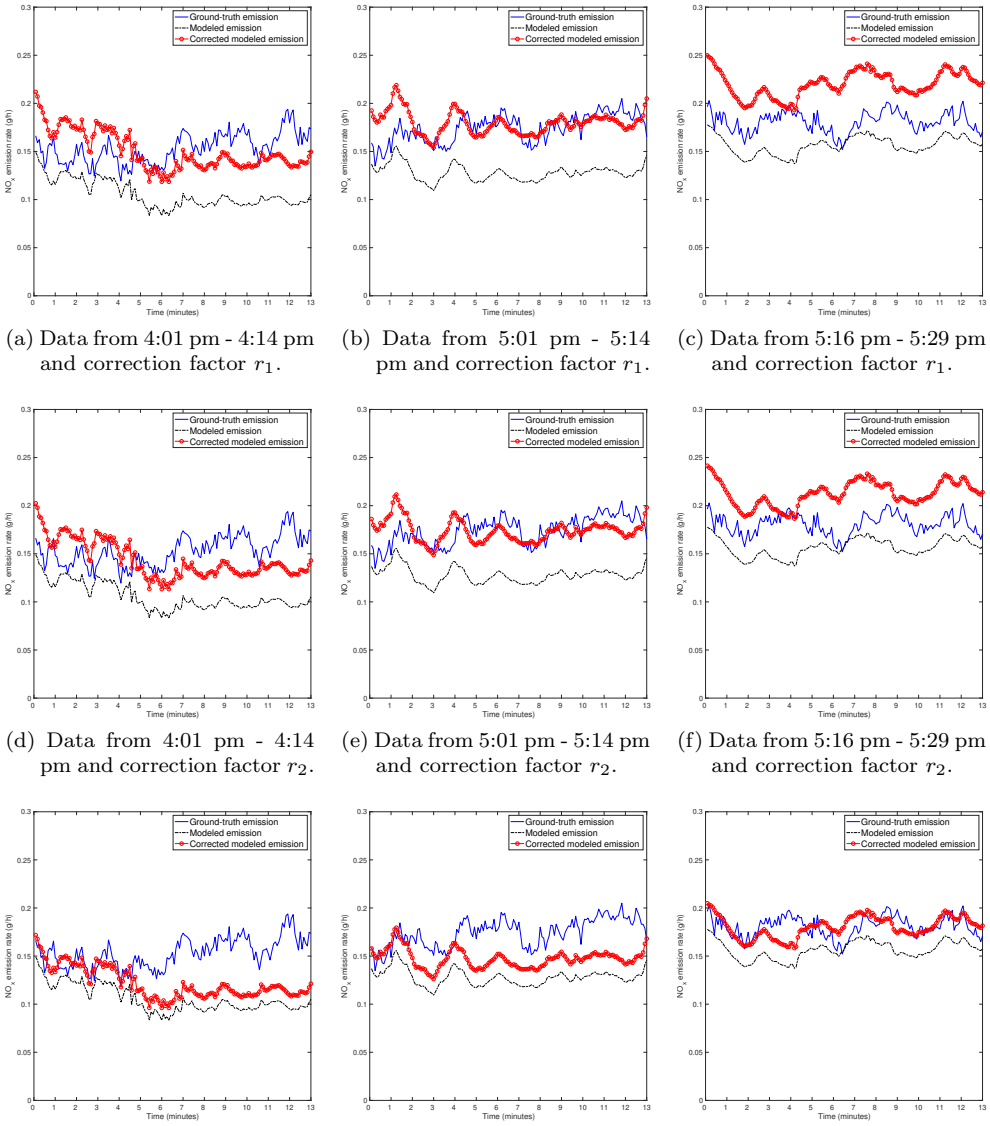

(a) Data from 4:01 pm - 4:14 pm and correction factor r_1.

(b) Data from 5:01 pm - 5:14 pm and correction factor r_1.

(c) Data from 5:16 pm - 5:29 pm and correction factor r_1.

(d) Data from 4:01 pm - 4:14 pm and correction factor r_2.

(e) Data from 5:01 pm - 5:14 pm and correction factor r_2.

(f) Data from 5:16 pm - 5:29 pm and correction factor r_2.

(g) Data from 4:01 pm - 4:14 pm and correction factor r_3.

(h) Data from 5:01 pm - 5:14 pm and correction factor r_3.

(i) Data from 5:16 pm - 5:29 pm and correction factor r_3.

Figure 3. Comparison of modeled (black-dotted), modeled with correction factors r_j (red-circles) and ground-truth (blue-solid) emission rates along 500 meters of road during 13 minutes of simulation for the three time periods of the NSGIM dataset. The top row is computed for $r_1 = 1.42$, the central row for $r_2 = 1.35$ and the bottom row for $r_3 = 1.15$.

6.2 Applications of Algorithm 1

Let us consider the CGARZ traffic model (2.2) on a time horizon $[0, T]$ and on a road with one lane parametrized by $[0, L]$. We fix the maximum speed $V^{\max} = 120\,\text{km/h}$, maximum density $\rho^{\max} = 133\,\text{veh/km}$ and left boundary condition $\rho(0, t) = 42\,\text{veh/km}\ \forall t$, while we use Neumann boundary condition on the right, which corresponds to allowing all vehicles to leave the road. The other parameters used in all simulations are $T = 30\,\text{min}$, $L = 10\,\text{km}$, $\Delta x = 0.1\,\text{km}$, $\Delta t = 0.5\Delta x/V^{\max}$ and the initial density $\rho_0 = 42\,\text{veh/km}$ in the first $4.5\,\text{km}$ of the road and $\rho_0 = 110\,\text{veh/km}$ otherwise.

In the following we show different traffic scenarios to evaluate the production of ozone using the procedure described in Algorithm 1.

6.2.1 Traffic dynamic 1: road without traffic lights

The dynamic is described by an initial shock wave around the middle of the road and a rarefaction wave stemming from the right end of the road. The shock wave propagates backward for the first 10 minutes, when the interaction with the rarefaction wave, and the consequent cancellation, changes the shock speed to positive. In Figure 4 we compare the 3D plots of density, speed, acceleration and NO_x emission rates. The four graphs have the same shape, since they depend on the density of vehicles. The acceleration reaches the minimum value along the blue curve shown in the graph, while the maximum value is reached at the beginning of the simulation at the end of the road, when the vehicles leave the road with maximum flux. Finally, the NO_x emission rate has a peak in correspondence of the highest values of acceleration and it is equal to 0 along the curve with the darkest blue.

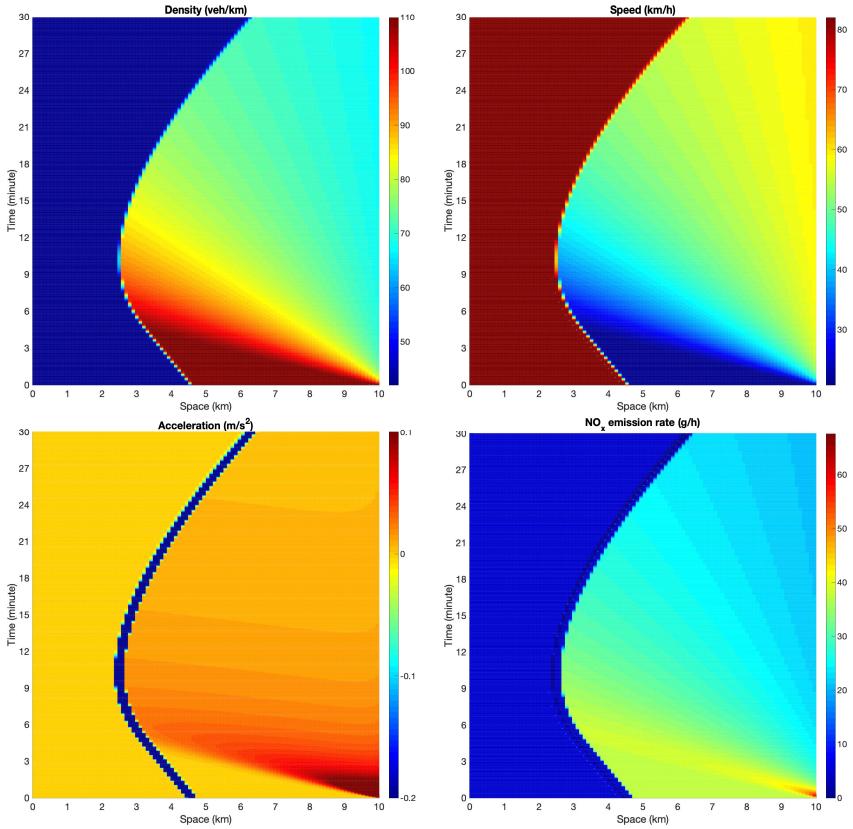

Figure 4. Traffic dynamic 1: Variation of density (top-left), speed (top-right), analytical acceleration (bottom-left) and NO_x emissions (bottom-right) in space and time.

On the left plot of Figure 5 we show data points of speed, acceleration and emission obtained along the numerical test. More precisely, the horizontal and vertical axes denote speed and acceleration, respectively, while the color gives the NO_x emission value. We observe that the NO_x emission is higher for positive value of the acceleration and low speed, and it decreases with negative acceleration. On the right plot of Figure 5 we show the variation in time of the total emission, defined as the sum on the cells of the emission rates, at any time. For this test, the total emission increases until the dynamics is described by the shock wave, and then it starts to decrease.

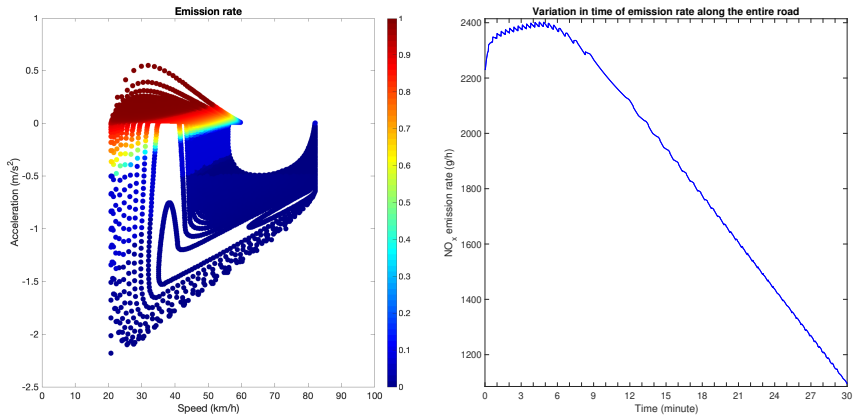

Figure 5. Traffic dynamic 1: NO_x emission rate as a function of speed and acceleration (left); variation in time of the total emission rate along the entire road (right).

6.2.2 Traffic dynamic 2: road with traffic lights

Here we test the effect of different traffic light cycles varying the time frame of the red phase. The latter corresponds to a Neumann boundary condition imposing vanishing outflow, while the green phase correspond to Neumann boundary condition allowing all cars to leave the road. We start by showing the solution obtained with a traffic light cycle of 5 minutes with a 2 minutes red phase. In Figure 6 we show density, speed, acceleration and NO_x emission rate in space and time. The wave with high density created by the red traffic lights takes about 18 minutes to reach the left boundary of the road. Once it reaches the left boundary of the road we see a periodic behavior in all the graphs, determined by the traffic lights. The graphs related to density and speed have opposite behavior: when the density increases the speed decreases and vice versa. Similar to test Traffic dynamic 1, the acceleration reaches the maximum values when the traffic light turns green and the vehicles leave the road. Again, the peaks of NO_x emission rates correspond to the highest acceleration values.

In Figure 7 we show on the left the emission rate as a function of speed and acceleration, and on the right the total emission along the road in time. Similar to Figure 5, the left graph shows higher emission levels at positive acceleration, but also at low speed and values of acceleration near to $-0.5\,\mathrm{m/s^2}$. In the graph we can see two phases, horizontally divided at height -0.5. We observe that $-0.5\,\mathrm{m/s^2}$ is the acceleration value which distinguishes the two possible choices of the parameters in (3.1), see Table 1. The right graph of Figure 7 shows the total emission in time, where the red and green lines represent the relative traffic light. We observe that, during the first 20 minutes, the emission rate increases faster when the traffic light is green and slower when it is red. Then, it reaches a maximum value after which it assumes a periodic behavior which depends on the traffic light.

Let now $r = t_g/t_r$ be the ratio between the time t_g of the green phase and the time t_r of the red phase respectively, and let t_c be the time of the whole traffic light phase, i.e. $t_c = t_g + t_r$. We consider two different test cases: first we fix the ratio r and we vary the time t_c; then, conversely we fix t_c and we vary r.

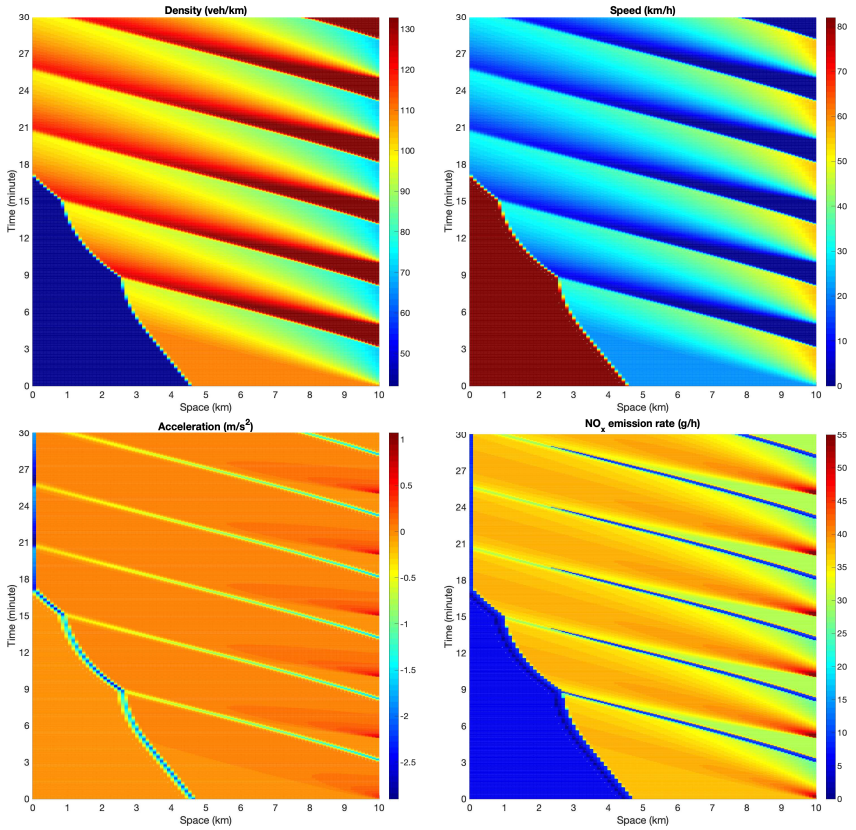

Figure 6. Traffic dynamic 2: Variation of density (top-left), speed (top-right), analytical acceleration (bottom-left) and NO_x emissions (bottom-right) in space and time.

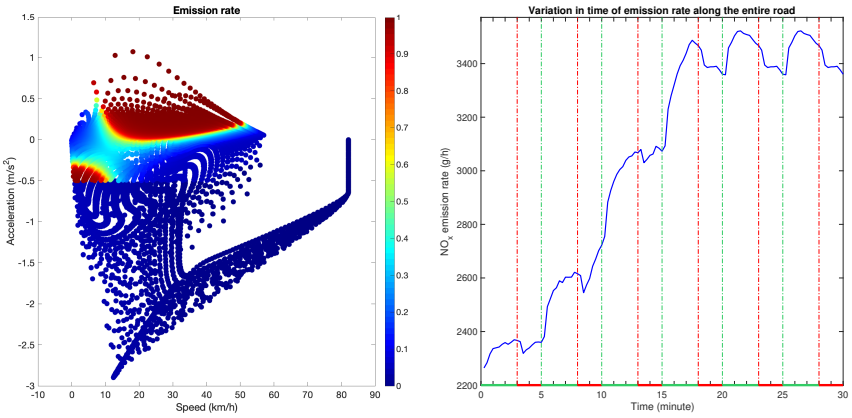

Figure 7. Traffic dynamic 2: NO_x emission rate as a function of speed and acceleration (left); variation in time of the total emission rate along the entire road (right).

Traffic dynamic 2.1: Emissions when the ratio r is constant. In Figure 8 we show the NO_x emissions obtained with $r = 3/2$ and three different values of traffic light duration in minutes: on the left we set $t_c = 7.5$ and $t_r = 3$, in the center $t_c = 5$ and $t_r = 2$ and on the right $t_c = 2.5$ and $t_r = 1$. We observe that the maximum value of the NO_x emission rate increases when the frequency of vehicles restarts augments, namely when the time t_r of the red phase is lower.

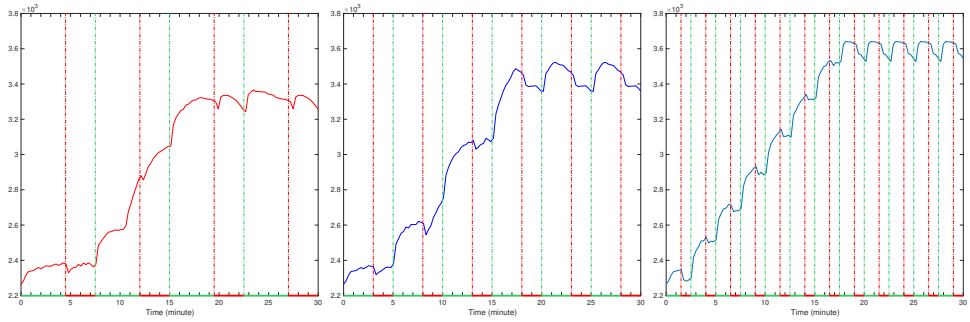

Figure 8. Traffic dynamic 2.1: Variation in time of the total NO_x emission rate along the entire road with $r = 3/2$ and varying the traffic light duration t_c in minutes: $t_c = 7.5$ with $t_r = 3$ (left); $t_c = 5$ with $t_r = 2$ (center); $t_c = 2.5$ with $t_r = 1$ (right).

Traffic dynamic 2.2: Emissions when the traffic light duration t_c is constant. In Figure 9 we show how the NO_x emissions vary with different ratio r. Specifically, we plot NO_x total emissions (defined as the sum on the cells of the emission rates, at any time) for one hour of simulation with $r = \{4,\ 3/2,\ 2/3\}$ which is equivalent to assume $(t_g, t_r) = (4\,,1\,)$, $(t_g, t_r) = (3\,,2\,)$, $(t_g, t_r) = (2\,,3\,)$ in minutes, respectively. We observe that until $t_r \leq t_g$ (solid line and line with circle) the maximum of the emission rate increases when t_r grows, since the are more vehicle restarts; while it decreases with $t_r > t_g$ (line with stars) when there are less vehicles restarts and more phases of stopped traffic.

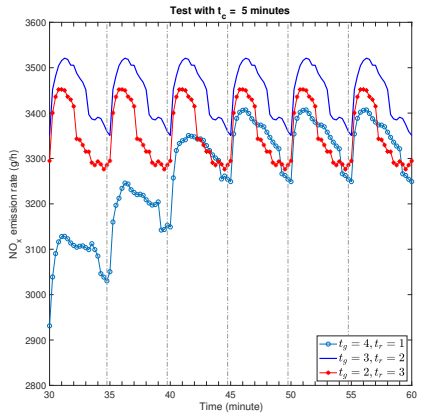

Figure 9. Traffic dynamic 2.2: Variation in time of the total emission rate along the entire road varying the ratio r.

To sum up, the two last examples developed in Traffic dynamic 2.1 and Traffic dynamic 2.2, suggest that the emissions grow with the increase of vehicles restarts. In particular, we observe from Figure 8 that the length of the traffic light cycle t_c has an highly influence on emissions, while Figure 9 shows that the ratio r between red-light and green-light has a less effect on the asymptotic emission values.

6.2.3 Production of ozone

In this section we are interested in estimating the concentration of ozone along the entire road by means of the system (4.5). The reaction rate parameters k_1, k_2 and k_3 are listed in Table 2. For each cell x_j, $j = 1, \dots, N_x$, we set the initial concentrations $\{\psi_i(x_j, 0)\}_{i=1,\dots,5}$ as $\psi_1(x_j, 0) = \psi_3(x_j, 0) = 0$, $\psi_2(x_j, 0) = 5.02 \times 10^{18}$ molecule/cm^3 and, according to Section 4 and relation (4.4), for NO and NO_2 we have

$$\psi_4(x_j, 0) = (1 - p)\frac{E_{NO_x}(0)}{\Delta x^3}, \quad \psi_5(x_j, 0) = p\frac{E_{NO_x}(0)}{\Delta x^3} \quad \text{with } p = 0.15.$$

For each time step n and for each x_j, we compute the source term due to traffic by using the emission rate given in Traffic dynamic 1 and Traffic dynamic 2.

In Figure 10, we show the O_3 evolution along the entire road, during half an hour of simulation. We observe a behaviour amenable to the traffic variables dynamics given in Figures 4-6. To obtain now the total concentration of all the chemical species along the entire road, for every time t^n we sum the results on all the cells. In Figure 11 we show the variation in time of the concentration of O_3 and O_2. We observe that the ozone concentration has a huge growth (Traffic dynamic 1 - blue-solid line), which is further amplified by the presence of the traffic light (Traffic dynamic 2 - red-circles line). On the other hand, the oxygen concentration is almost constant in both the cases, with moderated dependence on traffic light.

To further investigate the impact of the traffic light on all the chemical species concentration, we solve our system starting from the NO_x emission rates computed in Traffic dynamic 2.1 in which we fix the ratio r constant. Thus, we compute the total amount of O_3, NO, NO_2 and O, obtained during the whole simulation along the entire road. Then, we measure the variation of each concentration with respect to the one obtained in the test case without traffic light Traffic dynamic 1. The results in Table 4 show that all the concentrations increase coherently with the behavior of the NO_x source term, see Figure 8. So, we can conclude that the duration of traffic cycles affects all the chemical species production more than the ratio between green and red phase.

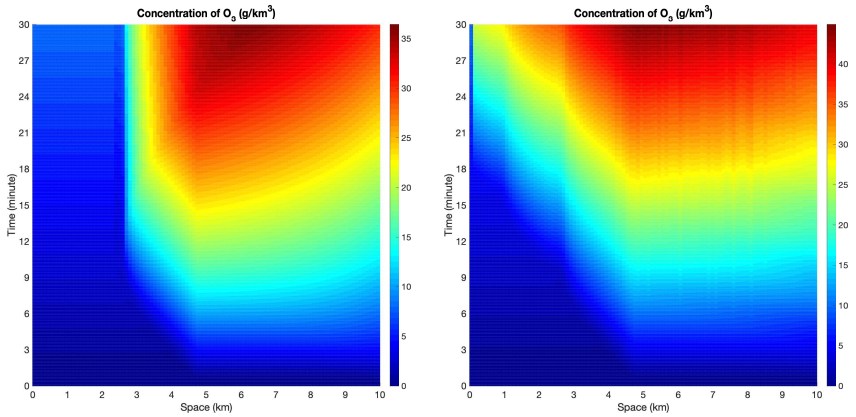

Figure 10. O_3 evolution along the entire road, for half an hour of simulation, in the case of dynamics without (left) and with (right) traffic light.

7 Conclusions

In this paper we proposed to couple a second-order model for traffic with a simplified system of reactions in the atmosphere for ozone production. The coupling is obtained via a general emission model, with parameters specifically tuned on NO_x pollutants. Via numerical simulations we tested various traffic scenarios obtaining three main results: 1) acceleration waves are most responsible for

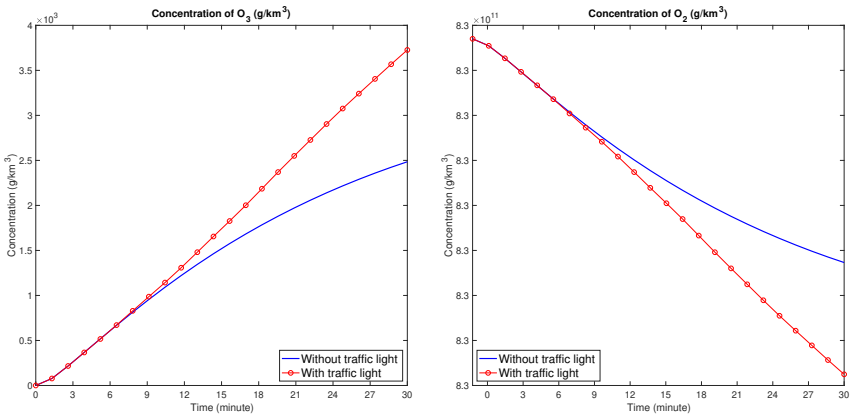

Figure 11. Variation in time of the total concentration of O_3 (left) and O_2 (right), in the case of dynamics with (red-circles) and without (blue-solid) traffic light.

$t_c = t_r + t_g$	$(3 + 4.5)$ min	$(2 + 3)$ min	$(1 + 1.5)$ min
O_3	4.26e+05	4.92e+05	5.75e+05
NO	5.64e+06	6.53e+06	7.67e+06
NO_2	1.73e+05	2.02e+05	2.42e+05
O	0.49	0.54	0.59

Table 4. Variation of the total amount of O_3, NO, NO_2 and O concentration (g/km^3) computed with three different traffic light duration (Traffic dynamic 2.1) with respect the total amount of concentrations without traffic light (Traffic dynamic 1).

NO_x emissions; 2) the length of traffic cycles impact emissions more than the ratio between green and red light; 3) ozone production is strongly impacted by traffic with linear growth regimes in presence of traffic light. Future investigations will include extending the model to networks, to more complex chemical phenomena and incorporating diffusion and transportation effects on emissions.

Acknowledgements

B.P.'s work was supported by the National Science Foundation under Cyber-Physical Systems Synergy Grant No. CNS-1837481. C.B. and M.B. would like to thank the Italian Ministry of Instruction, University and Research (MIUR) to support this research with funds coming from PRIN Project 2017 (No. 2017KKJP4X entitled "Innovative numerical methods for evolutionary partial differential equations and applications").

References

[1] L. J. Alvarez-Vázquez, N. García-Chan, A. Martínez, and M. E. Vázquez-Méndez, *Numerical simulation of air pollution due to traffic flow in urban networks*, J. Comput. Appl. Math., 326 (2017), pp. 44–61.

[2] R. Atkinson, *Atmospheric chemistry of* VOCs *and* NO_x, Atmos. Environ., 34 (2000), pp. 2063–2101.

[3] R. Atkinson and W. P. Carter, *Kinetics and mechanisms of the gas-phase reactions of ozone with organic compounds under atmospheric conditions*, Chem. Rev., 84 (1984), pp. 437–470.

[4] A. Aw and M. Rascle, *Resurrection of "Second Order" Models of Traffic Flow*, SIAM J. Appl. Math., 60 (2000), pp. 916–944.

[5] M. Barth, F. An, T. Younglove, G. Scora, C. Levine, M. Ross, and T. Wenzel, *Development of a comprehensive modal emissions model: Final report*, tech. rep., National Research Council, Transportation Research Board, National Cooperative Highway Research Program, NCHRP Project 25-11, 2000.

[6] D. C. Carslaw, S. D. Beevers, J. E. Tate, E. J. Westmoreland, and M. L. Williams, *Recent evidence concerning higher* NO_x *emissions from passenger cars and light duty vehicles*, Atmos. Environ., 45 (2011), pp. 7053–7063.

[7] D. de la Fuente, J. M. Vega, F. Viejo, I. Díaz, and M. Morcillo, *Mapping air pollution effects on atmospheric degradation of cultural heritage*, J. Cult. Herit., 14 (2013), pp. 138–145.

[8] European Environment Agency, *Air quality in europe – 2019 report*, tech. rep., 2019.

[9] S. Fan, M. Herty, and B. Seibold, *Comparative model accuracy of a data-fitted generalized Aw-Rascle-Zhang model*, Netw. Heterog. Media, 9 (2014), pp. 239–268.

[10] S. Fan, Y. Sun, B. Piccoli, B. Seibold, and D. B. Work, *A Collapsed Generalized Aw-Rascle-Zhang Model and its Model Accuracy*, arXiv preprint arXiv:1702.03624, (2017).

[11] M. Garavello, K. Han, and B. Piccoli, *Models for Vehicular Traffic on Networks*, American Institute of Mathematical Sciences, 2016.

[12] D. J. Jacob, *Heterogeneous chemistry and tropospheric ozone*, Atmos. Environ., 34 (2000), pp. 2131–2159.

[13] M. Z. Jacobson, *Fundamentals of Atmospheric Modeling*, Cambridge University Press, 2005.

[14] J. D. Lambert, *Numerical methods for ordinary differential systems*, John Wiley & Sons, Ltd., Chichester, 1991.

[15] J.-P. Lebacque, S. Mammar, and H. Haj-Salem, *Generic second order traffic flow modelling*, in Transportation and Traffic Theory, Elsevier, 2007, pp. 755–776.

[16] T. Luspay, B. Kulcsar, I. Varga, S. K. Zegeye, B. De Schutter, and M. Verhaegen, *On acceleration of traffic flow*, in Proceedings of the 13th International IEEE Conference on Intelligent Transportation Systems (ITSC 2010), IEEE, 2010, pp. 741–746.

[17] S. Manahan, *Environmental chemistry*, CRC press, 2017.

[18] H. Omidvarborna, A. Kumar, and D.-S. Kim, NO_x *emissions from low-temperature combustion of biodiesel made of various feedstocks and blends*, Fuel Process. Technol., 140 (2015), pp. 113 – 118.

[19] L. I. Panis, S. Broekx, and R. Liu, *Modelling instantaneous traffic emission and the influence of traffic speed limits*, Sci. Total Environ., 371 (2006), pp. 270–285.

[20] B. Piccoli, K. Han, T. L. Friesz, T. Yao, and J. Tang, *Second-order models and traffic data from mobile sensors*, Transp. Res. Part C Emerg. Technol., 52 (2015), pp. 32 – 56.

[21] V. Ramanathan, *Air pollution, greenhouse gases and climate change: Global and regional perspectives*, Atmos. Environ., 43 (2009), pp. 37–50.

[22] M. Rössler, T. Koch, C. Janzer, and M. Olzmann, *Mechanisms of the* NO_2 *formation in diesel engines*, MTZ Worldw., 78 (2017), pp. 70–75.

[23] S. Samaranayake, S. Glaser, D. Holstius, J. Monteil, K. Tracton, E. Seto, and A. Bayen, *RealTime Estimation of Pollution Emissions and Dispersion from Highway Traffic*, Comput.-Aided Civ. Inf., 29 (2014), pp. 546–558.

[24] J. H. Seinfeld and S. N. Pandis, *Atmospheric chemistry and physics: from air pollution to climate change*, John Wiley & Sons, 2016.

[25] R. Smit, L. Ntziachristos, and P. Boulter, *Validation of road vehicle and traffic emission models – a review and meta-analysis*, Atmos. Environ., 44 (2010), pp. 2943 – 2953.

[26] F. Song, J. Y. Shin, R. Jusino-Atresino, and Y. Gao, *Relationships among the springtime ground–level* NO_x*,* O_3 *and* NO_3 *in the vicinity of highways in the US East Coast*, Atmos. Pollut. Res., 2 (2011), pp. 374–383.

[27] J. M. Stockie, *The mathematics of atmospheric dispersion modeling*, SIAM Rev., 53 (2011), pp. 349–372.

[28] J. Tidblad, K. Kreislová, M. Faller, D. de la Fuente, T. Yates, A. Verney-Carron, T. Grøntoft, A. Gordon, and U. Hans, *ICP Materials Trends in Corrosion, Soiling and Air Pollution (1987–2014)*, Materials (Basel), 10 (2017).

[29] Transportation Research Board, *Critical issues in transportation 2019*, tech. rep., The National Academies of Sciences, Engineering, Medicine, 2019.

[30] TRB Executive Committee, *Special Report 307: Policy Options for Reducing Energy and Greenhouse Gas Emissions from U.S. Transportation*, tech. rep., Transportation Research Board of the National Academies, 2011.

[31] US Department of Transportation and Federal Highway Administration, *Next Generation Simulation (NGSIM)*. http://ops.fhwa.dot.gov/trafficanalysistools/ngsim.htm.

[32] T. Wang, L. Xue, P. Brimblecombe, Y. Lam, L. Li, and L. Zhang, *Ozone pollution in China: A review of concentrations, meteorological influences, chemical precursors, and effects*, Sci. Total Environ., 575 (2017), pp. 1582–1596.

[33] R. P. Wayne, *Chemistry of atmospheres*, Clarendon Press, Oxford, 1991.

[34] S. Zegeye, B. De Schutter, J. Hellendoorn, E. Breunesse, and A. Hegyi, *Integrated macroscopic traffic flow, emission, and fuel consumption model for control purposes*, Transp. Res. Part C Emerg. Technol., 31 (2013), pp. 158–171.

[35] H. M. Zhang, *A non-equilibrium traffic model devoid of gas-like behavior*, Transp. Res. B, 36 (2002), pp. 275–290.

[36] K. Zhang and S. Batterman, *Air pollution and health risks due to vehicle traffic*, Sci. Total Environ., 450-451 (2013), pp. 307 – 316.